ARTICLE

Check for updates

Cleaner burning aviation fuels can reduce contrail cloudiness

Christiane Voigt [1,2 ✉], Jonas Kleine[1,2], Daniel Sauer[1], Richard H. Moore [3], Tiziana Bräuer [1], Patrick Le Clercq [4], Stefan Kaufmann[1], Monika Scheibe[1], Tina Jurkat-Witschas[1], Manfred Aigner[4], Uwe Bauder [4], Yvonne Boose [1], Stephan Borrmann[2,5], Ewan Crosbie[3], Glenn S. Diskin [3], Joshua DiGangi[3], Valerian Hahn[1,2], Christopher Heckl[1], Felix Huber[1], John B. Nowak [3], Markus Rapp [1,6], Bastian Rauch [4], Claire Robinson[3], Tobias Schripp [4], Michael Shook [3], Edward Winstead[3], Luke Ziemba[3], Hans Schlager[1] & Bruce E. Anderson[3]

Contrail cirrus account for the major share of aviation's climate impact. Yet, the links between jet fuel composition, contrail microphysics and climate impact remain unresolved. Here we present unique observations from two DLR-NASA aircraft campaigns that measured exhaust and contrail characteristics of an Airbus A320 burning either standard jet fuels or low aromatic sustainable aviation fuel blends. Our results show that soot particles can regulate the number of contrail cirrus ice crystals for current emission levels. We provide experimental evidence that burning low aromatic sustainable aviation fuel can result in a 50 to 70% reduction in soot and ice number concentrations and an increase in ice crystal size. Reduced contrail ice numbers cause less energy deposition in the atmosphere and less warming. Meaningful reductions in aviation's climate impact could therefore be obtained from the widespread adoption of low aromatic fuels, and from regulations to lower the maximum aromatic fuel content.

[1] Deutsches Zentrum für Luft- und Raumfahrt (DLR), Oberpfaffenhofen, Germany. [2] Johannes Gutenberg-University, Mainz, Germany. [3] NASA Langley Research Center, Hampton, VA, USA. [4] Deutsches Zentrum für Luft- und Raumfahrt (DLR), Stuttgart, Germany. [5] Max-Planck-Institute for Chemistry, Mainz, Germany. [6] Ludwig-Maximilians-University, München, Germany. ✉email: Christiane.Voigt@dlr.de

Aircraft engines emit a variety of combustion products including 3.16 kg of carbon dioxide (CO_2) and about 1.23 kg of water vapour (H_2O) for every kg of fuel burned[1]. At the cold temperatures that are typical of cruise altitudes, the H_2O rapidly condenses onto co-emitted soot particles and pre-existing atmospheric particles. The small water droplets continue to grow in size as the engine exhaust plume cools until they eventually freeze, forming a visible line-shaped condensation trail, or contrail, that consists of several hundred ice crystals per cubic centimetre of air[2–5]. The persistence of this newly-formed contrail is governed by the ambient temperature and H_2O mixing ratio. An ice supersaturated environment sustains the contrail for some hours, allowing it to grow and spread to form extended contrail cirrus over regional scales[6,7]. Indeed, such features are commonly detected from space[8,9], which highlights their potential importance for altering the Earth's radiation budget by scattering incoming solar radiation back into space (cooling the Earth), by extinguishing solar radiation and depositing solar energy into the atmosphere (warming the atmosphere) and by trapping outgoing infrared radiation (warming the Earth). Overall, the net effect of contrail cirrus clouds on climate is thought to be warming[10,11], with a global average effective radiative forcing of 57 mW m^{-2} and a 90% likelihood range of 17–98 mW m^{-2} [1]. Thus, contrail cirrus yields the largest single contribution to the net effective radiative forcing from aviation of 101 mW m^{-2} in 2018[1], followed by the contributions from aircraft CO_2 and NO_x emissions.

While the globally averaged contribution of air traffic to anthropogenic climate forcing is ~3.5%[1], the regional fingerprint of contrail cirrus on the atmospheric energy budget can be significantly higher. For example, in major air traffic corridors over the United States and Europe, contrail cirrus may warm the atmospheric column by more than 500 mW m^{-2}, and hence contribute substantially to the regional anthropogenic radiative forcing[12,13]. Also, air traffic has increased markedly in the last two decades, resulting in an increase in effective radiative forcing from contrail cirrus by 64% from 2005 to 2018[1]. The surface warming of contrail cirrus is expected to further increase in the future with some projections suggesting a 3–4-fold increase by the year 2050[14,15]. Growing air traffic also leads to substantial greenhouse gas emissions. However, unlike long-lived CO_2, contrail cirrus only exist in the atmosphere for a period of hours[7], which means that efforts to reduce contrail cirrus would have an immediate cooling effect on climate. Multiple mitigation strategies are currently being considered, including weather-dependent flight routing[16] or cruise altitude variations to avoid contrail cirrus formation[17]; however, some of these approaches may come at the cost of increased fuel burn, longer flights, or reduced airspace capacity. In addition to measures for avoiding contrail formation in the first place, the next best strategy might be to reduce the radiative impact of the clouds that do form.

Global model simulations suggest that a reduction in the contrail cirrus radiative forcing could be achieved by decreasing the ice crystal number concentration[18]. One possible mechanism, supported by theory[19], that could be used to achieve this goal is to change the jet fuel composition to reduce the soot particle emissions. Previous flight campaigns[20] demonstrated that the use of a jet biofuel blends reduced soot number emissions at cruise altitudes. Despite these promising results, a direct link between soot number and contrail ice crystal number has not been established experimentally for those biofuels. Indeed, there has even been some suggestion that the enhanced fuel hydrogen content of the jet biofuel might actually promote rather than suppress the contrail forcing because of the increased H_2O emissions[20]. Resolving these questions takes on additional urgency as national and international organizations seriously consider the use of alternative bio-based jet fuels and fuel blends for reducing the aviation CO_2 emissions coming from fossil fuels[21,22]. Recent advances at international level suggest sustainable aviation fuels in order to reduce aviation's non-CO_2-climate impact to zero by 2050[23]. Here, we report the results of in-flight testing under contrail-forming conditions that further constrain the effects of alternative fuel blends on aircraft soot emissions and directly connect these particle emissions to the properties of the resulting contrail cirrus clouds (Fig. 1). The Deutsches Zentrum für Luft- und Raumfahrt (DLR) and the National Aeronautics and Space Administration (NASA) collaborated on two recent flight campaigns wherein instrumented research aircraft sampled the exhaust plume and contrail behind the DLR Advanced Technology Research Aircraft (ATRA). A photo of the NASA DC-8 chasing the contrail of the ATRA is shown in Fig. 1. The ATRA is a state-of-the-art Airbus A320 equipped with two International Aero Engines V2527-A5 engines and a comprehensive suite of sensors to capture the real-time, in-flight aircraft performance data. The flight tests were carried out as part of the Emission and Climate Impact of Alternative Fuel (ECLIF) project with the first set of flights conducted in 2015 (ECLIF1) with the DLR Falcon 20 sampling aircraft from Oberpfaffenhofen, Germany, and the second set of flights conducted in 2018 (ECLIF2/ND-MAX) with the NASA DC-8 sampling aircraft operating from Ramstein Air Base, near Kaiserslautern, Germany. Both campaigns also included comprehensive sets of ground tests to quantify the ATRA emissions data over the full aircraft landing and take-off cycle[24].

In flight contrail and emissions data were acquired for five different fuels, including two traditional, petroleum-based Jet A1 fuels (Ref2, and Ref3) and three blends of Jet A1 with synthetic jet fuel or bio-based alternative jet fuel. The distinction between the

Fig. 1 The NASA DC8 research aircraft probing contrails from the DLR A320 burning sustainable aviation fuel blends. Photo showing the DC8 chasing a contrail from the A320 burning a sustainable aviation fuel blend above Germany on 24 January 2018.

semisynthetic jet fuel blend (SSF1) and the sustainable aviation jet fuel blends (SAF1, and SAF2) is that the former uses the Fischer-Tropsch (FT) process to produce the synthetic kerosene component from coal while the latter contains a more sustainable, bio-based hydrotreated esters and fatty acids (HEFA) kerosene produced from plant oil.

Incomplete combustion of fuel hydrocarbon compounds in the aircraft engine leads to the emission of copious small spherical carbonaceous soot particles. Aviation fuel contains a major fraction of aliphatic hydrocarbon chain structures and <25% of cyclic aromatic hydrocarbons. Higher energies are required to break the chemical bonds and oxidize the aromatic rings compared to the hydrocarbon chains, therefore aromatics have been identified as major soot precursors[25,26]. Due to their ring structure, aromatic molecules exhibit a lower hydrogen to carbon ratio (H:C ~ 1:1) compared to aliphatic hydrocarbon chains (H:C ratios ~2:1). Hence, the fuel hydrogen content or the H:C ratio is a good measure for the sooting tendency of a fuel[24,27]. Naphthalenes are bi-cyclic aromatic hydrocarbons, whose role in soot formation is not yet known[24]. Here, we evaluate the hypothesis that naphthalenes are more efficient soot precursors than monocyclic aromatic molecules or hydrocarbon chain structures in the fuel.

The fuels were designed and blended to investigate the effects of aromatics and specifically naphthalene in alternative fuel blends[28] on soot particle emissions and ice particle formation in contrails. In addition, the sulfur content of the sustainable aviation fuels (see Table 1) was kept low to explore the influence of the changing hydrogen content while controlling for the sulfur effects on soot particle activation and volatile particle formation.

For ECLIF1, petroleum-based standard Jet A1 fuel with slightly <19% aromatic content by volume was blended with FT-based synthetic kerosene to produce the semisynthetic jet fuel blend SSF1 with 11.1% aromatics by volume. For the second flight experiment, two different Jet A1 fuels (Ref3 and Ref4) with different aromatic and naphthalene contents were blended with HEFA-based kerosene to produce sustainable aviation fuels (SAF1 and SAF2) with 8.5 and 9.5% aromatic content (by volume). To gain insight into the specific effects of poly-cyclic aromatic molecules in alternative fuel blends, SAF2 was prepared to contain 0.05% bi-cyclic naphthalenes by volume, which is more

than an order of magnitude lower than the naphthalene content the other blended test fuels. Indeed, even though SAF2 is 70% Jet A1 (by volume), it exhibits the highest hydrogen content of all the fuels tested. The measured fuel composition characteristics are summarized in Table 1. Here, we focus on the three alternative fuel blends to understand their emissions characteristics and impact on contrail properties relative to the Ref2 Jet A1 fuel.

Results and discussion

During the test flights, the A320 and sampling aircraft initially transited to reserved air space over Germany, where they entered a two-aircraft formation with the A320 flying oval race track patterns at constant air speed (0.58–0.76 Mach) and level flight altitude (8–12 km) while the sampling aircraft performed multiple exhaust plume and contrail crossings at <50 km trailing distances. During ECLIF1, the DLR Falcon sampling aircraft measured the contrail ice particle number concentrations using a Cloud and Aerosol Spectrometer Probe (CAS[29]), and the data were analyzed using the methodology defined in previous work[5]. For ECLIF2/ND-MAX, the DC-8 sampling aircraft used a Fast Forward Scattering Spectrometer Probe (FFSSP[30,31]) for the contrail measurements. In both campaigns, number concentrations of nonvolatile particles were measured with condensation particle counters modified for airborne application[32]. Detailed information on instrumentation and data evaluation is given in the Methods section.

To study the effects of fuels on contrail characteristics, we focus on time periods during the two missions where conditions were favorable for persistent contrail formation. On 22 September and 7 October 2015 during ECLIF1, temperatures at cruise altitudes were 5–9 °C below the Schmidt-Appleman temperature (SAT[33]), which is the threshold temperature below which contrails can thermodynamically occur. Similar conditions occurred during ECLIF2/ND-MAX on 23 and 24 January 2018, where persistent contrails were produced by the A320 at cruise levels between 9.7 and 10.7 km altitude and at temperatures of −53 to −58 °C. The DC-8 chasing the A320 contrail is shown in Fig. 1. The minutes-old contrails were measured in 7–41 km trailing distance behind the A320. Ambient conditions and their local variations for the analyzed contrail sequences are given in Table 2.

Table 1 Properties of fuels burned during the ECLIF1 and ECLIF2/ND-MAX experiments.

ECLIF fuels	Ref1	Ref2	Ref3	Ref4	SSF1	SAF1	SAF2
Fuel composition	100% Jet A1	100% JetA-1	100% Jet A1	100% Jet A1	59% Ref1+ 41% FT-SPK	51% Ref3+ 49% HEFA-SPK	70% Ref4 +30% HEFA-SPK
Aromatics (vol%) (ASTM D6379) SASOL/ Petrolab	**18.8** (±2.5)	**17.2** (±2.5)	**18.6** (±2.5)	**16.5** (±2.5)	**11.4** (±2.5)	**8.5** (±1.5)	**9.5** (±1.5)
Naphthalenes (vol%) (ASTM D1840)	**1.51** (±0.07)	**1.83** (±0.08)	**1.17** (±0.06)	**0.13** (±0.02)	**0.82** (±0.05)	**0.61** (±0.04)	**0.045** (±0.01)
Hydrogen content (mass%) (NMR ASTM D7171)	**13.67** (±0.14)	**13.73** (±0.08)	**13.65** (±0.05)	**14.08** (±0.18)	**14.36** (±0.02)	**14.40** (±0.07)	**14.51** (±0.04)
H:C ratio (NMR ASTM D7171)	**1.89** (±0.02)	**1.90** (±0.01)	**1.88** (±0.01)	**1.95** (±0.02)	**2.00** (±0.01)	**2.00** (±0.01)	**2.02** (±0.01)
Specific Energy (MJ/kg) (ASTM D3338)	**42.80** (±0.02)	**43.20** (±0.02)	**43.14** (±0.01)	**43.34** (±0.01)	**43.50** (±0.02)	**43.63** (±0.01)	**43.63** (±0.01)
Sulfur Total (mass%) (ASTM D2622) SASOL/ Petrolab	**0.117** (±0.003)	**0.135** (±0.003)	**0.012** (±0.001)	**<0.001** (±0.001)	**0.057** (±0.002)	**0.007** (±0.001)	**<0.001** (±0.001)

Fuel properties (± uncertainties according to certification standards) for fuels used for the contrail observations during ECLIF1 and ECLIF2/ND-MAX. Four reference fuels (Ref1 to Ref4), the semisynthetic jet fuel blend SSF1 and the sustainable aviation fuel blends SAF1 and SAF2 were probed in flight and/or in ground tests. Ref1 and Ref4 fuels were only included in the ground tests and were used for creating the alternative fuel blends. At similar atmospheric conditions, contrails were only observed on Ref2 fuel and on the alternative fuel blends SSF1, SAF1 and SAF2. Aromatics were determined by gas chromatography according to certification standard[56] ASTM D7566 by SASOL and Petrolab, the sulfur content was determined by SASOL for ECLIF1 and by Petrolab for ECLIF2/ND-MAX according to standard[57] ASTM D2622. Other components were measured by DLR, bi-cyclic naphthalenes according to certification standard method[58] ASTM D1840. The hydrogen content and the H:C ratio were measured using nuclear magnetic resonance relaxometry according to the standard[55] ASTM D7171 standard. Fuel properties were measured in the laboratory after the flight tests.

Table 2 Ambient conditions and engine settings during contrail measurement sequences.

Contrail measurement conditions	Ref 2	SSF1	SAF1	SAF2
Contrail age (s)	39–132	48–134	53–140	41–116
Sampling time (s)	482	280	284	119
Ambient RHI (%)	115-25 (±7)	108-15 (±10)	120 (±4)	110 (±5)
Ambient T (K)	215 (±0.5)	220 (±0.5)	218 (±0.5)	216 (±0.5)
T difference to SAC (K)	−9.0 (±0.5)	−4.9 (±0.5)	−5.9 (±0.5)	−8.0 (±0.5)
Altitude of source aircraft (m)	10670 (±5)	10364 (±3)	9726 (±3)	9656 (±2)
Fuel flow (kg/h) per engine	1180 (±30)	820 (±44)	1132 (±25)	1091 (±20)
N1 (%) thrust setting	81 (±1)	71 (±1)	77 (±0.6)	77 (±0.6)
Speed of source aircraft (Mach)	0.65 (±0.02)	0.58 (±0.01)	0.76 (±0.01)	0.76 (±0.01)

Measurement conditions for contrails with ages between 39 and 140 s at ambient RHI > 100%. The contrails had formed on emissions from the A320 burning the reference fuel Ref2, the semisynthetic jet fuel blend SSF1 or the sustainable aviation fuel blend SAF1 or SAF2. Ambient temperature at the altitude of the source aircraft (± instrumental uncertainty) and the temperature difference to the Schmidt-Appleman threshold temperature for contrail formation (SAC); the relative humidity with respect to ice determined with a frost point hygrometer for Ref2 and SSF1 (ECLIF-1) and with the diode laser hygrometer DLH for SAF1 and SAF2 (ECLIF2/ND-MAX) and their range ±50 m from the flight level. Fuel flow and thrust settings in % fan speed N1 with arithmetic standard deviation (± a.s.d.), speed of the aircraft with absolute deviations.
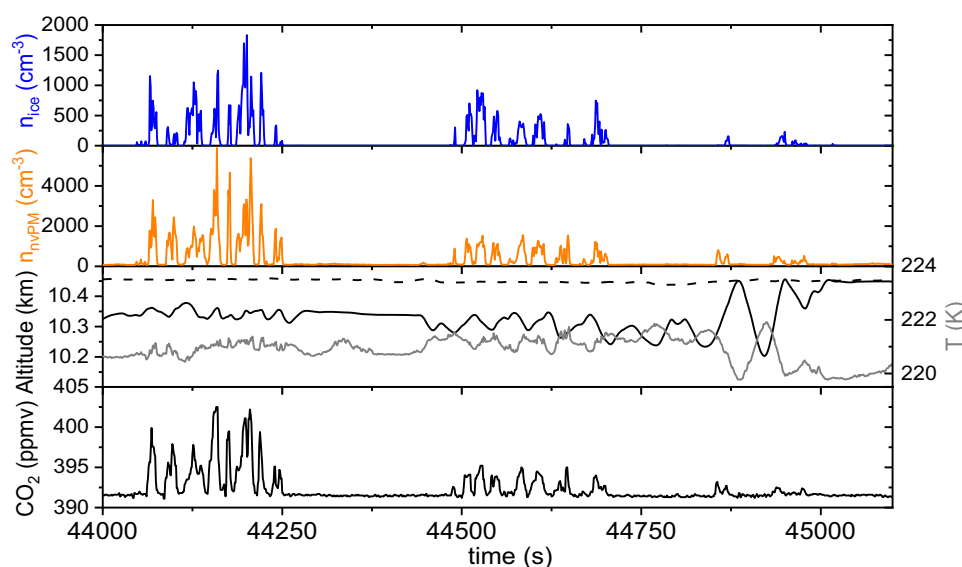

Fig. 2 Time series of 1-Hz data measured in the A320 contrail when burning low-aromatic semisynthetic jet fuel SSF1. Number concentrations of ice crystals with diameters larger than 0.5 μm (n_{ice}), nonvolatile (i.e., soot) particles in the size range of 0.01–1.9 μm (n_{soot}), altitude of Falcon (solid black line) and A320 (dashed black line), ambient temperature (gray line) and CO_2 mixing ratio. Measurements were taken at contrail ages from 48 to 134 s and distances between 7 and 41 km.

Figure 2 shows an example of the time series data collected by the DLR Falcon as it repeatedly crossed the A320 contrail. The crossings are evident by the large enhancements in ice crystal and nonvolatile particle number concentration as well as CO_2 mixing ratio relative to very stable background levels. The decreasing size of the peaks over time is due to the increasing separation distance between the two aircraft (10, 15.7, and 20.3 km), corresponding to older plume age and greater plume dilution. To achieve independence from dilution processes, the emission index, EI_x, of species x is derived from individual exhaust or contrail crossings and quantifies the amount of that species (i.e., number of ice or soot particles) emitted per kilogram of fuel burned under the assumption that the fuel carbon content is completely converted to CO_2 (see Methods). The apparent contrail ice emission index AEI_{ice} is also calculated in a similar manner; although, we use the term 'apparent' to recognize that the ice particles themselves are not directly emitted by the engines, but are connected to the engine fuel burn through the emitted exhaust particles.

For the Ref2 fuel, the measured nonvolatile particle emission index of $(4.9 \pm 0.6) \times 10^{15}$ soot particles produced per kilogram of

Jet A1 fuel burned is toward the upper end of the soot emission levels of the current aircraft fleet (10^{14}–10^{16} soot particles per kilogram of fuel burned[5,19,34]). The apparent ice emission index AEI_{ice} of $(4.2 \pm 0.6) \times 10^{15}$ ice particles per kilogram of fuel burned indicates that about 80–100% of the emitted soot particles are activated into contrail ice crystals (Table 3). Ubiquitous tiny volatile particles[35,36] have a minor impact on ice nucleation in the soot-rich regime and for low fuel sulfur content (see Table 1). This finding is consistent with theoretical expectations that soot particles regulate the number of contrail ice crystals and that background or small volatile particles do not significantly contribute to ice crystal formation for the observed conditions of high soot emissions (>10^{15} soot particles per kg-fuel) in the soot-rich regime and ambient temperatures well below the SAT[19,37]. Soot number emissions were consistently large (>3×10^{15} per kg-fuel) for the probed reference Jet A1 fuels.

In contrast, significantly lower soot and apparent ice particle emissions were measured in flight when the A320 burned the alternative fuel blends. Soot emissions indices for the HEFA-based sustainable aviation fuel blends are ~45–53% lower than
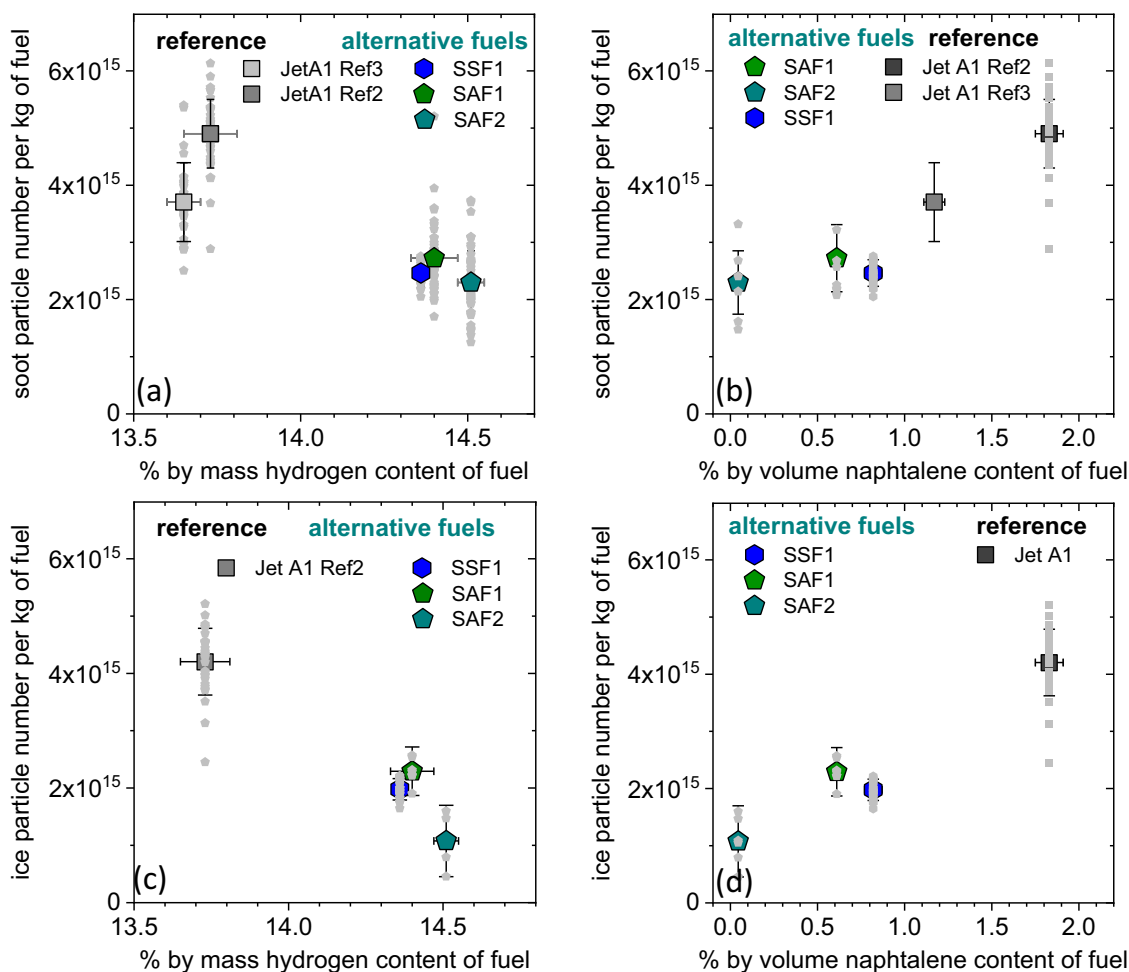
Fig. 3 Non-volatile (i.e., soot) and apparent ice particle emissions per kg of fuel at cruise conditions for the reference Jet A1 fuels and for the low-aromatic sustainable aviation fuel blends. a and **b** Nonvolatile particle emissions per kg of fuel for the reference Jet A1 fuels (Ref2, Ref3, dark gray and black), and for the low-aromatic fuel blends: the Fischer-Tropsch-based semisynthetic fuel blend SSF1 (blue), and the HEFA-based sustainable aviation fuel blends SAF1 (green) and SAF2 (cyan), (**c**) and (**d**) same for apparent ice emission indices AEI$_{ice}$; soot and apparent ice emissions are shown with respect to hydrogen content and bi-cyclic naphthalene content of the fuel blends. Arithmetic mean soot and ice particle emissions indices (±1 arithmetic standard deviation a.s.d.; (the uncertainty for AEI$_{ice}$ for SAF1 and SAF2 refers to the range of the observations (AEI$_{ice,min}$ to AEI$_{ice,max}$) due to lower data statistics, see Table 3); gray symbols are individual data points from exhaust and contrail crossings versus the fuel hydrogen content and fuel naphthalene content. Contrails have not been observed for Ref3 fuel. High hydrogen and low naphthalene sustainable aviation fuel blends reduce soot number emissions and apparent ice number emissions in contrails.

the Ref2 Jet A1 fuel consistent with[20]. We demonstrate here for the first time that the cruise soot emission index for the FT-based semisynthetic jet fuel also exhibits reductions of ~50%. These substantial soot particle reductions lead to 45–74% lower ice crystal apparent emission indices (EI) for the alternative jet fuel blends compared to the Ref2 Jet A1 fuel (Fig. 3). Of the blended fuels, the most significant soot emissions and ice crystal reductions are observed for the SAF2 fuel, which was specifically designed to have a similar aromatic content to the other alternative fuel blends but a different sooting hydrocarbon family composition, i.e., a higher hydrogen content of the Ref4 used for blending and an order of magnitude lower naphthalene content of the blend. This results in the SAF2 fuel having both the highest fuel hydrogen content and the lowest naphthalene content leading to lowest soot and ice emissions of all the tested fuels (Fig. 3). The results imply that bi-cyclic naphthalenes are more efficient soot precursors than mono-cyclic aromatic or aliphatic hydrocarbon structures.

We restricted the contrail data evaluation to ambient mean RHIs between 108 and 125% RHI, (Table 2). The SAF2 contrail was detected at the lower side of this humidity range at 110(±5)% RHI of contrails. The low and variable RHI for this contrail event might explain the reduced ice active fraction of SAF2 and a stronger ice crystal loss in contrails[5,38]. The error bars given in Fig. 3 are standard deviations of the individual contrail datasets, resulting from low number of contrail crossings for the SAF2 fuel. Further, the sustainable aviation fuel SAF2 with the lowest naphthalene content also has an undetectably low sulfur content. A summary of fuel composition and related emissions indices for reference Jet A1 fuel, for low-aromatic semisynthetic (SSF1) or sustainable aviation fuel blends (SAF1 and SAF2) is given in Table 3.

Comprehensive campaigns have investigated the role of fuel sulfur on exhaust particles[36]. Strong changes in the fuel sulfur content led to changes in volatile particle size rather than particle number[37,39]. Volatile particle numbers were further reduced in contrail conditions due to scavenging on the larger ice crystals. An impact on ice numbers in contrails could not be inferred[36,40].

Separating the contributions to contrail formation of the larger non-volatile soot particles and the smaller, volatile, non-soot-containing particles requires plume-scale modeling

Table 3 Summary of fuel composition and measured emissions indices for reference Jet A1 fuel (Ref2) and for low-aromatic semisynthetic (SSF1) or sustainable (SAF1 and SAF2) aviation fuel blends derived during the contrail measurement sequences at medium cruise thrust conditions.

Fuel type	Ref2 (Δ)	SSF1 (Δ)	SAF1 (Δ)	SAF2 (Δ)	Ref3 (Δ)
Aromatics (vol%) (ASTM D6379)	**17.2** (± 2.5)	**11.4** (± 2.5)	**8.5** (± 1.5)	**9.5** (± 1.5)	**18.6** (± 2.5)
Naphthalenes (vol%) (ASTM D1840)	**1.83** (± 0.08)	**0.82** (± 0.05)	**0.61** (± 0.04)	**0.05** (± 0.01)	**1.17** (± 0.06)
Hydrogen (mass%) (ASTM D7171)	**13.73** (± 0.08)	**14.36** (± 0.02)	**14.40** (± 0.07)	**14.51** (± 0.04)	**13.65** (± 0.05)
Nonvolatile particle number Emission Index ($D_p > 10$ nm) (kg-fuel^{-1})	(**4.9** $\pm$ 0.6) $\times 10^{15}$	(**2.5** $\pm$ 0.2) $\times 10^{15}$	(**2.7** $\pm$ 0.6) $\times 10^{15}$	(**2.3** $\pm$ 0.6) $\times 10^{15}$	(**3.8** $\pm$ 0.9) $\times 10^{15}$
Apparent ice crystal number Emission Index (AEI$_{ice}$) (kg-fuel^{-1})	(**4.2** $\pm$ 0.6) $\times 10^{15}$	(**2.0** $\pm$ 0.2) $\times 10^{15}$	(**2.3** $\pm$ 0.2) $\times 10^{15}$	(**1.1** $\pm$ 0.4) $\times 10^{15}$	
Number of plume intercepts	29	23	46	53	30
Number of contrail intercepts	29	23	7	6	

Summary of fuel composition and emissions indices measured in 39–140 s old contrails at 9.7 to 10.7 km altitude in persistent contrail conditions. Engine settings were at medium-thrust cruise conditions and fuel flow rates as indicated in Data Table 1 and ambient conditions as detailed in Table 2. Ice particle and aerosol emissions indices are reported as the arithmetic mean ±1 arithmetic standard deviation (a.s.d.) as described in detail in methods. Ref3 parameters are given as reference for ECLIF2/ND-MAX, while contrails were not observed at comparable ambient conditions.
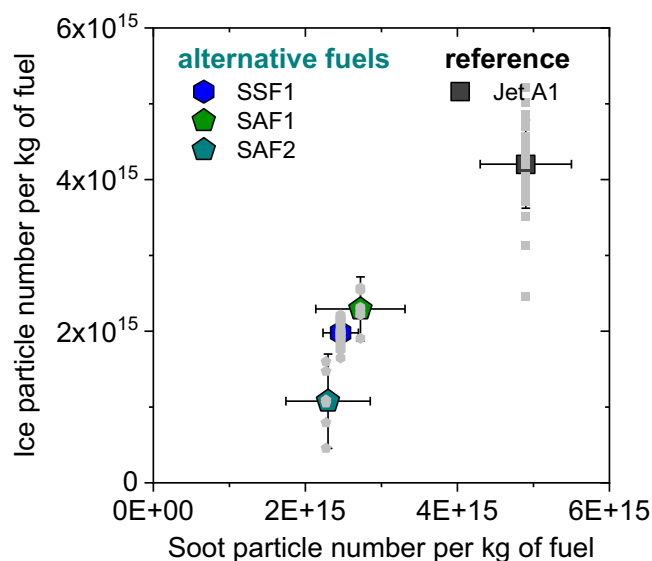

Fig. 4 Correlation between soot particle and apparent ice emission indices AEI$_{ice}$ for reference Jet A1 jet fuel, and for the low-aromatic sustainable aviation fuel blends. Arithmetic mean soot and ice particle emissions indices normalized to the fuel flow for the reference Jet A1 jet fuel Ref2 (black), for the semisynthetic fuel blend SSF1 (blue), and for the HEFA-based sustainable aviation fuel blends SAF1 (green) and SAF2 (cyan); (±1 arithmetic standard deviation a.s.d.; gray symbols are individual data points, the uncertainty for AEI$_{ice}$ for SAF1 and SAF2 refers to the range of the observations (AEI$_{ice,min}$ to AEI$_{ice,max}$) due to lower data statistics, see Table 3). Burning low aromatic aviation fuels results in reduced soot and ice number concentrations in contrails.
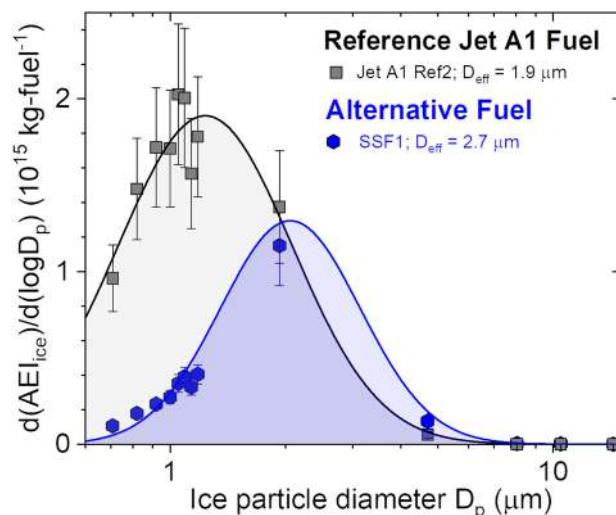

Fig. 5 Apparent ice emission index distribution with respect to contrail particle size from the reference Jet A1 fuel (Ref2, black) and from the low-aromatic semisynthetic jet fuel SSF1 (blue). The dilution-normalized ice size distributions AEI$_{ice}$ have been detected in 1 min-old contrails at corresponding wake depths; error bars give the combined error due to uncertainty in the CO_2 background level determination and the arithmetic standard deviation of bin mean values due to counting statistics. A lognormal distribution was fitted to the data (see Methods). While AEI$_{ice}$ decreases for the contrail nucleated when burning the Fischer-Tropsch based designer fuel SSF1, the effective contrail ice crystal diameter increases for SSF1 compared to the contrail that had nucleated on the reference Jet A1 fuel.

constrained by observations. Modeling work has shown that the Kelvin effect preferentially activates the larger (30–40 nm) soot particles[20,41] versus the smaller volatile particles[42]. Also, in the so-called 'soot-rich regime' exceeding 10^{15} kg^{-1} (see Fig. 4), the soot particles actively scavenge the sulfur oxidation products in the exhaust at the expense of volatile particles[19]. Hence, volatile particles emissions during ECLIF2/ND-MAX neither show a dependence on fuel hydrogen nor on the fuel sulfur content for the probed low sulfur fuels.

It's important to note that the small volatile particles or atmospheric background particles do begin to contribute meaningfully to contrail formation under 'soot-poor' regimes (<10^{13} soot particles per kg of fuel burned) that might result from

next-generation hydrogen fuels or lean-burn engine technology. This occurs because the low soot particle concentrations in the exhaust do not effectively scavenge the sulfur oxidation products and because the volatile aerosol grows to larger sizes at low ambient temperatures[19]. Fortunately, for the ECLIF/ND-MAX soot EIs in the 'soot-rich regime', we may reasonably neglect the contribution of the non-soot-containing particles to ice crystal numbers, which allows us to directly connect observed changes in EI$_{soot}$ to AEI$_{ice}$ for the first time.

In addition to the emissions reductions, size resolved AEI$_{ice}$ distributions of the contrails formed on standard and low-aromatic-content jet fuels help to interpret the observed reductions in contrail ice numbers (Fig. 5). The contrail ice size distribution formed on Jet

A1exhaust particles has an effective diameter of 1.9 μm[43]. The effective diameter of the ice crystals is 40% larger for the one-minute-old contrail with lower ice numbers formed from burning the alternative fuel, again relative to the same point in the Ref2 contrail (Fig. 5). While the increased hydrogen content of the semisynthetic fuel blend does result in a 4% increase to the engine's H_2O emissions (1.28 kg H_2O per kg of fuel), it has only a minor effect on the ice crystal size.

The increase in crystal size mainly occurs as the H_2O in the contrail condenses onto fewer contrail ice crystals, which had resulted from fewer soot particles being emitted from burning the alternative fuel blends. Only about a quarter of the contrail ice water content of 4.98 kg H_2O per kg of fuel measured in the 1 min-old contrail was emitted by the engines, the remainder had condensed from the supersaturated ambient atmosphere. Theoretical studies[18] show that the larger ice crystals sediment and sublimate faster and therefore contrails with reduced ice numbers have a shorter atmospheric lifetime.

Initial ice number concentrations in contrails are a key parameter for determining light extinction by contrails[44], and their climate impact[18]. Thereby, the amount of light extinction by a contrail is directly related to its capacity to deposit radiative energy in the atmosphere and thereby warm the ambient atmosphere[16]. In our case, the extinction of the 1 min-old SSF1 contrail is ~30% reduced with respect to the Jet A1 contrail. Simulations show that changes in initial ice numbers strongly impact the total extinction of contrails over hours[44]. Global model simulations[18] initialized with 50–90% reduced ice number concentrations in 7 min-old contrails show a non-linear reduction in the radiative forcing from contrail cirrus by 20–70%, mainly caused by the reduced initial ice numbers, and, in addition, by reduced contrail lifetime due to faster sedimentation of the larger ice crystals.

Hence, lower ice numbers as measured in the contrails from sustainable aviation fuel blends directly translate into reduced contrail extinction, reduced energy deposition in the atmosphere and reduced warming. This work closes the experimental gap between changes in aircraft fuel composition, mono- and poly-cyclic aromatic content of the fuel, aircraft engine soot emissions and the resulting contrail ice numbers and microphysical properties, which global models suggest as the most important drivers of aviation's climate footprint[1,16,18].

This means that the recent advances in lean-burn engine technologies and the development of sustainable, bio-based fuels for reducing soot emissions should contribute to lessening the regional and global climate impact of aviation. The targeted use of sustainable low aromatic jet fuels in contrail outbreak situations, that contribute substantially to the warming by contrail cirrus[16,18] can further increase the climate benefit from SAF.

The positive climate effect from sustainable aviation fuels is enhanced by their higher fuel energy content (see Table 1), which increases fuel efficiency and reduces fuel consumption. Also, the very low sulfur level of sustainable aviation fuel limits ice nucleation from volatile exhaust particles even in the soot-poor regime, when entrainment of background aerosol gains in importance.

Our results also highlight the promise of advanced jet fuel design as a method for further reducing these impacts and suggests that a targeted reduction of sooting hydrocarbon families such as poly-cyclic aromatics or cyclo-alkanes in aviation fuels in order to increase the fuel hydrogen content may achieve even stronger reductions of aircraft's soot emissions. This approach opens new options to design next-generation jet fuels in order to meet the international standards for standard or alternative jet fuels, while also reducing the radiation and climate impact of associated contrail cirrus clouds.

Methods

Source aircraft and engines. The DLR ATRA is an Airbus A320-232 (serial number 3C0C4B) equipped with two International Aero Engines IAE-V2527-A5 engines. The IAE-V2527-A5 mixed turbofan engine has a maximum rated thrust of 111.2 kN, a maximum pressure ratio of 27.2 and a bypass ratio of 4.82 representative for the V2500 family[24]. Compared to commercial aircraft it flies a low number of annual flight hours (<1000)[24]. The smoke number is 5.2 for take-off, 7.2 for climb out, 4.2 for approach and 2.6 for idle, see unique identification number 1IA003 as referenced in the ICAO emissions data bank v24.

Fuel certification and blending. International certification standards by ASTM International were used to analyze the fuels for this study as given in the references[24]. These include ASTM D1319, the Standard Test Method for Hydrocarbon Types in Liquid Petroleum Products by Fluorescent Indicator Adsorption, DOI: 10.1520/D1319-02A, ASTM D2622, the Standard Test Method for Sulfur in Petroleum Products by Wavelength Dispersive X-ray Fluorescence Spectrometry, DOI: 10.1520/D2622-16, ASTM D1840, the Standard Test Method for Naphthalene Hydrocarbons in Aviation Turbine Fuels by Ultraviolet Spectrophotometry, DOI: 10.1520/D1840-07R17 and ASTM D7171, the Standard Test Method for Hydrogen Content of Middle Distillate Petroleum Products by Low-Resolution Pulsed Nuclear Magnetic Resonance Spectroscopy, DOI: 10.1520/D7171-16[24].

A petroleum-based standard Jet A1 fuel (Ref1) from the NatRef refinery with 18.8% by volume aromatic content was blended by SASOL (South African Synthetic Oil Limited) with 41% by volume of a FT-based synthetic jet fuel to produce the semisynthetic jet fuel blend SSF1 with 11.4% by volume aromatic fuel content. The HEFA-based sustainable alternative jet fuel blends were produced by different refineries and blended by DLR with variable portions (51 and 70% by volume) of standard Jet A1 fuels with 18.6% by volume (Ref3) and 16.5% by volume (Ref4) aromatic content resulting in two HEFA-based sustainable alternative jet fuel blends with 8.5 (SAF1) and 9.5% by volume (SAF2) aromatic content. To gain insight into the effects of bi-cyclic aromatic molecules, the naphthalene content of Ref3 (1.17% by volume) was lowered to 0.61% by volume for SAF1 and 0.045% by volume for SAF2. In addition, the hydrogen content and the hydrogen to carbon molar ratios of the fuel blends were determined. The fuel composition is given in Table 1.

Conventional petroleum-based jet fuels (essentially kerosene) are highly refined and consist of a complex mixture of hydrocarbon species with 9 to more than 16 carbon atoms[28]. The standard specification for jet fuels containing synthetic hydrocarbons requires that the final blend (conventional fossil-based Jet A1 and up to 50 vol% synthetic blend) has a density of >760 kg m^{-3} and contains between 8 and 25% by mass of aromatic hydrocarbons[20]. Jet A1 fuels may contain up to 0.3% by mass of sulfur. In contrast, pure alternative fuels contain near-zero aromatics and only traces of sulfur, usually introduced during handling and shipping through Jet A1 contaminated fuel systems[45]. Alternative fuels are produced from a large variety of feedstocks e.g., coal, natural gas, biomass, waste, and renewable electricity and typically contain a much narrower spectrum of hydrocarbon species[28]. The FT process converts carbon monoxide and hydrogen gas mixtures into an alternative aviation fuel blend. The sustainability depends highly upon the CO_2 footprint of this production route. Hydro-processed Esters and Fatty Acid (HEFA) is an ASTM approved bio-based jet fuel blend, which is produced for example from used cooking oil, Camelina, or Jatropha plant oil[46].

Particle and trace gas measurements. Particles and trace gases were measured with a set of well characterized instruments that have been deployed aboard aircraft in previous campaigns[3,30]. The CAS[29] mounted under the wing of the Falcon was used during ECLIF1 to measure ice particle number concentrations and the size distribution in the contrails adapting the methodology from previous work[5]. Particles in the size range of 0.5–50 μm traverse the focus of a laser beam and the signal scattered in 4–12° forward direction is detected by a photodetector. The CAS was size-calibrated[47,48] leading to uncertainties of ±16% for ice particle diameters (D_p) reported here. Ice crystals with larger sizes contribute <1% to the total ice number concentrations in contrails[3] and are not discussed further. Ice particle shattering[49] was not observed during the contrail penetrations, as expected for low concentrations of large ice crystals. A CAS sampling area of 0.21 mm^2 was determined by laboratory calibrations. An empirical coincidence correction function was derived[5] and was used to correct the CAS data for coincidence effects. A 10% correction was added to the contrail ice particle numbers to correct for ice particles <0.5 μm, which are not measured by the CAS.

During ECLIF2/ND-MAX the FFSSP-300 (Fast Forward Scattering Spectrometer Probe) was mounted at 62° on the upper fuselage of the DC-8 to measure ice particle concentrations in the vicinity of the CO_2 inlet, which was used to calculate EI. The low-drag configuration of the FFSSP's housing compared to the CAS allowed its installation near the CO_2 inlet on the DC8's fuselage. In addition, its location in proximity to the aerosol inlet facilitates the comparison of ice and aerosol measurements. The probe measures particles in a size range between 0.8 and 25 μm. Particles crossing the focus of an open path He-Ne laser beam with a wavelength of 632.8 nm scatter light and the light scattered into the angular range of 3–15° is detected by a photodetector[30]. The sampling area of 0.19 mm^2 was mapped using a mono-dispersed stream of water droplets. The probe received an electronic update in 2017 and now records data from single particles. The FFSSP

was also size-calibrated[47,48] on the basis of a T-Matrix calculation for an ice particle aspect ratio of 0.5. The ice number concentrations reported here comprise only particles with sizes larger than 1 μm to due to instrumental noise in the lowest channel. Based on particle size distribution data in contrails measured by the CAS, an effective diameter dependent correction factor between 1.1 and 1.4 was applied to the FFSSP data to account for smaller ice crystals.

Number concentrations of nonvolatile particles were measured with condensation particle counters (CPCs) based on TSI, Model 3010 counters (TSI, Inc, USA), modified and optimized for airborne application. During ECLIF1 they were connected to a forward-facing near-isokinetic aerosol inlet. Number concentration of nonvolatile particles were determined by sampling from a sample line heated to 250 °C to evaporate volatile components of the total aerosol. The remaining non-volatile aerosol components are assumed to be predominantly composed of soot. During near-field measurements (ECLIF1) the sample flow was diluted by a factor of 30 using an inline dilution system to avoid saturation of the particle counters. CPC data have been corrected for reduced detection efficiencies in low pressure environments[50] and particle losses in the Thermodenuder. We determine an overall uncertainty in nonvolatile particle number concentrations of ±15%. The evaluation of nonvolatile particles data for ECLIF1 is described in detail[5]. During ECLIF2/ND-MAX aerosol particles were sampled using a central, "scoop"-style aerosol inlet sampling non-isokinetically at high flows. While this inlet is designed to deflect larger cloud droplets and ice particles away from the aerosol sampling line, small contrail ice particles can enter the inlet and sublimate such that the majority of soot residuals are detectable in the particle counters.

Carbon dioxide (CO_2) was measured using a cavity ring down spectroscopy (CRDS) instrument manufactured by Picarro Inc., Santa Clara, CA, USA (model: G2301-m flight analyzer). For CO_2 detection, a laser emits pulses into a three-mirror cavity with the wavelength of a CO_2 absorption line. The time required to attenuate the pulses in the cavity is proportional to the mole fraction of CO_2 in the sample air. The cavity is operated at a constant pressure of 140 Torr. The pressure stability is achieved by using a pump in the sample air inlet line and by regulating the inlet valve of the cavity. The effect of H_2O on the CO_2 reading is corrected during post-processing of the data[51]. The precision (2 s) of the CO_2 measurements is 0.1 ppmv. The accuracy is 0.3 ppmv and can be traced back to the NOAA/ESRL (Earth System Research Laboratory/ Global Greenhouse Gas Reference Network) CO_2 calibration standard. The CO_2 signal rise time (10–90%) and fall time (90–10%) is 1.5 s. The measurement interval is 2.0 s. Sample air was passed to the CRDS instrument via a backward-facing inlet mounted to the upper part of the fuselage of the Falcon and DC8.

During ECLIF1, H_2O mixing ratios were measured with an uncertainty of ±7% with a CR-2 frost point hygrometer from Buck Research Instruments, LLC[3,52] connected to a backward-facing inlet to exclude sampling of condensed water. The meteorological measurement system onboard the Falcon detected temperature and pressure with accuracies of ±0.5 K and ±0.5 hPa, respectively. From the H_2O and temperature data, the ambient relative humidity with respect to ice (RHI) was calculated. In the air surrounding the contrails RHI ranged between 107 and 125% on days when contrails formed with an estimated uncertainty of ±7–10%.

During ECLIF2/ND-MAX the NASA Langley Diode Laser Hygrometer (DLH) provided H_2O measurements aboard the DC-8 with high temporal resolution[53]. The DLH is an open path airborne tunable diode laser-based instrument, which operates in the near-infrared spectral region at a wavelength of ~1.39 μm. The DLH measures the H_2O mixing ratio in the atmosphere by wavelength modulated differential absorption spectroscopy. Its laser is modulated at ~2000 Hz and operates in a 'line-locked' mode; the signal is demodulated at twice the modulation frequency (2F detection) to provide good sensitivity and rapid time response. Ambient pressure and temperature, measured separately on the aircraft, are used to convert normalized 2F signal to H_2O mixing ratio. Due to the large range of H_2O concentration in the atmosphere from percent-level concentrations at or near sea level to a few parts per million in the lower stratosphere, the DLH operates on one of three spectral absorption lines, and switches automatically among them depending on measured signal levels. The open path on the NASA DC-8 is formed between a laser transceiver, located in the cabin, and a piece of commercially available road-sign-type retroreflector sheeting affixed to the nacelle of the outboard port-side engine. The total, round-trip optical path is ~28.5 m.

Atmospheric cruise conditions. Semisynthetic jet fuel SSF1 (Ref2) was burned in both engines of the ATRA on the flights on 22 September (7 October) 2015. The thermodynamic threshold temperature for contrail formation[33] of 224–225 (±0.7) K for the flights was calculated from the meteorological data assuming an overall propulsion efficiency of 0.3. The contrails were probed at 9.0 K (Ref2) and 4.9 K (SSF1) below this temperature threshold.

Sustainable alternative jet fuel SAF1 and SAF2 was burned in both engines of the ATRA during the flights on 23 and 24 January 2018, respectively. The contrails were probed at 5.9 K (SAF1) and 8 K (SAF2) below the contrail temperature threshold. Further information on ambient conditions and engine settings are given in Table 2. Measurements in the far field at distances larger than 7 km are necessary to overcome sampling challenges of the particle probes caused by saturation effects due to coincident transmission of two or more particles through

the sampling volume[54]. At those distances, the counter rotating wake vortices induced by the wing tips may mix and emissions from the two engines cannot be separated by in-situ measurements. The age of the contrail at each penetration sequence was derived by analyzing GPS flight track data of source aircraft (ATRA) and measurement platforms (Falcon, DC-8) taking into account the wind drift.

$$\mathrm{AEI_{ice}} = \left(\frac{\Delta N_{ice}}{\Delta CO_2}\right) \cdot \left(\frac{M_{air}}{M_{CO_2} \cdot \Delta\rho_{air}}\right) \cdot \mathrm{EI_{CO2}} \qquad (1)$$

Calculation of emissions indices. To account for dilution or mixing with ambient air as well as inhomogeneities in the exhaust, the data are analyzed in terms of EI, relating particle or gas concentrations to the mass of fuel burnt. This value is assessed indirectly via the CO_2 measurement by scaling particle and trace gas measurements to CO_2 with a known and constant CO_2 emission index. Here a unique value for CO_2 of $EI_{CO2} \approx 3.160$ g kg^{-1} is used, the slightly enhanced hydrogen contents of the alternative fuel blends. This introduces an error <1% (+0.13% for Ref2 and −0.6% for SSF1) in the calculation of the emission index, which is included in the experimental uncertainties. For non-volatile aircraft-generated particles, EI gives the number of particles emitted per unit mass of fuel consumed. As particles are not directly emitted by the engines, the term apparent ice particle emission index AEI_{ice} is used. With this concept, soot and ice particle numbers can directly be compared. Particle number EI are calculated[45] as ratios of enhancements in particle number concentrations above their respective background (ΔN) to the simultaneously measured CO_2 enhancement (ΔCO_2) by with the molar masses of air (M_{air}), CO_2 (M_{CO2}), and the density of air ρ_{air}. ΔN_{ice} is the integrated ice number density and ΔCO_2 the integrated CO_2 mixing ratio over individual contrail sequences.

Apparent ice emission indices at the engine exit. By juxtaposing vertical profiles of soot and ice particle EI, previous work[5] finds an anti-correlation caused by the sublimation of ice particles in the descending and adiabatically heated primary vortices, as expected from theory[44]. Here we use the same strategy for the reference Jet A1 and SSF data measured during ECLIF1. Measured AEI_{ice} and EI_{soot} are summed up to calculate the vertical profile of the particle emission index (soot and ice) from these observations. AEI_{ice} and EI_{soot} respective to engine exit conditions are then derived from the contrail profile using the activated fraction of the total particles[5]. AEI_{ice} and EI_{soot} were evaluated at single-engine fuel flow rates of 1180 ± 100 kg hr^{-1} in order to constrain the dependence of EI on fuel flow. EI from SSF1 were measured at single-engine fuel flow rates of 820 ± 44 kg hr^{-1}. Ground data show an increase of 15% in EI_{soot} for the higher fuel flow rates[24], therefore EI of SSF were scaled by 15% to account for differences in fuel flow rates.

A different aerosol inlet was used during ND-MAX, which precludes the implementation of this approach for ECLIF2/ND-MAX data. Therefore, we derive the AEI_{ice} near the engine exit for the SAF fuel blends directly from ice particle observations ±50 m above and below the flight altitude of the source aircraft. Close to the source aircraft, unaccounted ice particle losses due to sublimation may cause an uncertainty of 10%.

Apparent ice emission index size distribution. The dilution-normalized ice size distributions AEI_{ice} (Fig. 5) have been detected in the 58 s-old SSF1 contrail and in 66 s-old Jet A1 contrail at corresponding wake depths Δz of 99 m (SSF1) and 100 m (Ref2). EI from SSF1 were again scaled by 15% to account for differences in fuel flow rates with respect to Jet A1. Total AEI_{ice} are 10.5 (±2.2) *10^{14} for the contrail nucleated on the reference Jet A1 fuel and 6.7 (±1.5) *10^{14} kg^{-1} for the SSF1 contrail, the effective diameter of 1.9 μm for the reference Jet A1 contrail increases to 2.7 μm for the contrail nucleated on emissions from low-aromatic semisynthetic jet fuel.

Ice particle emissions index distributions over the particle size range from 0.5 to 25 μm measured by the CAS were fitted using a log-normal function of the form

$$\frac{d(\mathrm{AEI_{ice}})}{d[\log(D_p)]} = \frac{n_{Dp}}{\sqrt{2\pi}\sigma D_p}\exp\left\{-\frac{\left[\log\left(\frac{D_p}{D_c}\right)\right]^2}{2\sigma^2}\right\} \qquad (2)$$

where D_p is the ice particle diameter, n_{Dp} is the total ice particle number per kg-fuel in the diameter interval D_p, D_c is the geometric mean diameter of the distribution and σ is related to the distribution width. Fit coefficients are $D_c = 2.46$ (±0.11) μm; $\sigma = 0.42 \pm 0.02$ and $n_{Dp} = 3.08 (\pm 0.21)\times 10^{15}$ for the SSF1 with the fit quality given by the coefficient of determination R^2 (COD) of 0.97; and $D_c = 1.61$ (±0.10) μm; $\sigma = 0.52 \pm 0.04$ and $n_{Dp} = 3.51 (\pm 0.22)\times 10^{15}$ for the Ref[2] Jet A1 fuel with R^2 (COD) of 0.974.

Data availability
The datasets for this study are available in the DLR data repository at https://halo-db.pa.op.dlr.de/ for the ECLIF1 data and from the NASA archive located at https://science-data.larc.nasa.gov/aero-fp/projects/ for ECLIF2/ND-MAX and from the corresponding author upon request.

References

1. D.S. Lee et al. The contribution of global aviation to anthropogenic climate forcing for 2000 to 2018. *Atmos. Environ.* **244**, https://doi.org/10.1016/j.atmosenv.2020.117834 (2021)
2. Heymsfield, A. et al. Contrail microphysics. *Bull. Am. Meteorol. Soc.* **91**, 465–472 (2010).
3. Voigt, C. et al. In-situ observations of young contrails—overview and selected results from the CONCERT campaign. *Atmos. Chem. Phys.* **10**, 9039–9056, https://doi.org/10.5194/acp-10-9039-2010 (2010).
4. Schumann, U. et al. Properties of individual contrails: a compilation of observations and some comparisons. *Atmos. Chem. Phys.* **17**, 403–438, https://doi.org/10.5194/acp-17-403-2017 (2017).
5. Kleine, J. et al. In situ observations of ice particle losses in a young persistent contrail. *Geophys. Res. Lett.* **45**, 553–13,561 (2018).
6. Minnis, P. et al. Linear contrail and contrail cirrus properties determined from satellite data. *Geophys. Res. Lett.* **40**, 3220–3226 (2013).
7. Vázquez-Navarro, M., Mannstein, H. & Kox, S. Contrail life cycle and properties from 1 year of MSG/SEVIRI rapid-scan images. *Atmos. Chem. Phys.* **15**, 8739–8749, https://doi.org/10.5194/acp-15-8739-2015 (2015).
8. Iwabuchi, H., Yang, P., Liou, K. N. & Minnis, P. Physical and optical properties of persistent contrails: climatology and interpretation. *J. Geophys. Res.: Atmos.* **117**, D06215 (2012).
9. Tesche, M., Achtert, P., Glantz, P. & Noone, K. J. Aviation effects on already-existing cirrus clouds. *Nat. Commun.* **7**, 12016 (2016).
10. Burkhardt, U. & Kärcher, B. Global radiative forcing from contrail cirrus. *Nat. Clim. Change* **1**, 54–58 (2011).
11. Stocker, T. et al. IPCC Climate Change *2013: The Physical Science Basis.* Contribution of WG I to the Fifth Assessment Report of the Intergovernmental Panel on Climate Change (IPCC) (eds. Stocker, T. F. et al.) (Cambridge University Press, 2013).
12. Bock, L. & Burkhardt, U. Reassessing properties and radiative forcing of contrail cirrus using a climate model. *J. Geophys. Res.: Atmos.* **121**, 9717–9736 (2016).
13. Schumann, U. A contrail cirrus prediction model. *Geosci. Model Dev.* **5**, 543–580, https://doi.org/10.5194/gmd-5-543-2012 (2012).
14. Bock, L. & Burkhardt, U. Contrail cirrus radiative forcing for future air traffic. *Atmos. Chem. Phys.* **19**, 8163–8174, https://doi.org/10.5194/acp-19-8163-2019 (2019).
15. Chen, C.-C. & Gettelman, A. Simulated 2050 aviation radiative forcing from contrails and aerosols. *Atmos. Chem. Phys.* **16**, 7317–7333 (2016).
16. Teoh, R., Schumann, U., Majumdar, A. & Stettler, M. E. J. Mitigating the climate forcing of aircraft contrails by small-scale diversions and technology adoption. *Environ. Sci. Technol.* **54**, 2941–2950, https://doi.org/10.1021/acs.est.9b05608 (2020).
17. Grewe, V. et al. Mitigating the Climate Impact from Aviation: achievements and Results of the DLR WeCare Project. *Aerospace*, **4**, https://doi.org/10.3390/aerospace4030034 (2017).
18. Burkhardt, U., Bock, L. & Bier, A. Mitigating the contrail cirrus climate impact by reducing aircraft soot number emissions. *npj Clim. Atmos Sci.* **1**, 37, https://doi.org/10.1038/s41612-018-0046-4 (2018).
19. Kärcher, B. Formation and radiative forcing of contrail cirrus. *Nat. Commun.* **9**, 1824, https://doi.org/10.1038/s41467-018-04068-0 (2018).
20. Moore, R. H. et al. Biofuel blending reduces particle emissions from aircraft engines at cruise conditions. *Nature* **543**, 411–415 10oi.1038/nature21420. (2017).
21. Savage, N. Fuel options: The ideal biofuel. *Nature* **474**, 9–10 (2011).
22. ICAO International Civil Aviation Organization fuels guide, https://www.icao.int/environmental-protection/knowledge-sharing/Docs/Sustainable%20Aviation%20Fuels%20Guide_vf.pdf. last accessed 18 Nov 2019 (2017).
23. Arrowsmith, S. Report from the Commission to the European Parliament and the Council: Updated analysis of the non-CO₂ climate impacts of aviation and potential policy measures pursuant to EU Emissions Trading System. *Directive Article* 30, MOVE/E1/SER/2019-475/SI2.817062, https://www.easa.europa.eu/sites/default/files/dfu/201119_report_com_ep_council_updated_analysis_non_co2_climate_impacts_aviation.pdf (2020).
24. Schripp, T. et al. Impact of alternative jet fuels on engine exhaust composition during the 2015 ECLIF ground-based measurements campaign. *Environ. Sci. Technol.* **52**, 4969–4978 (2018).
25. Lobo, P., Hagen, D. E. & Whitefield, P. D. Comparison of PM Emissions from a Commercial Jet Engine Burning Conventional, Biomass, and Fischer-Tropsch Fuels. *Environ. Sci. Technol.* **45**, 10744–10749 https://doi.org/10.1021/es201902e. (2011).
26. Brem, B. T. et al. Effects of Fuel Aromatic Content on Nonvolatile Particulate Emissions of an In-Production Aircraft Gas Turbine. *Environ. Sci. Technol.* **49**, 13149–13157 (2015).
27. Cain, J. et al. Characterization of Gaseous and Particulate Emissions from a Turboshaft Engine Burning Conventional, Alternative, and Surrogate Fuels. *Energy Fuels* **27**, 2290–2302 (2013).
28. Pregger, T. et al. Future Fuels—Analyses of the Future Prospects of Renewable Synthetic Fuels. *Energies* **13**, 138 (2020).
29. Baumgardner, D., Jonsson, H., Dawson, W., O'Connor, D. & Newton, R. The cloud, aerosol and precipitation spectrometer: a new instrument for cloud investigations. *Atmos. Res.* **59**, 251–264 (2001).
30. Voigt, C. et al. Extinction and optical depth of contrails. *Geophys. Res. Lett.* **38** https://doi.org/10.1029/2011GL047189 (2011).
31. Voigt, C. et al. ML-CIRRUS: The airborne experiment on natural cirrus and contrail cirrus with the High-Altitude Long-Range research aircraft HALO. *Bull. Am. Meteorol. Soc.* **98**, 271–288, https://doi.org/10.1175/BAMS-D-15-00213.1 (2017).
32. Feldpausch, P., Fiebig, M., Fritzsche, L. & Petzold, A. Measurement of ultrafine aerosol size distributions by a combination of diffusion screen separators and condensation particle counters. *Aerosol Sci.* **37**, 577–597 (2006).
33. Schumann, U. On conditions for contrail formation from aircraft exhausts. *Meteorologische Zeitschrift* **5**, 4–23 (1996).
34. Kärcher, B., Kleine, J., Sauer, D. & Voigt, C. Contrail formation: analysis of sublimation mechanisms. *Geophys. Res. Lett.* **45**, 547–13,552 (2018).
35. Brock, C. A. et al. Ultrafine particle size distributions measured in aircraft exhaust plumes. *J. Geophys. Res.* **105**, 26555–26567, https://doi.org/10.1029/2000JD900360 (2000).
36. Schumann, U. et al. Influence of fuel sulfur on the composition of aircraft exhaust plumes: the experiments SULFUR 1–7. *J. Geophys. Res.* **107**, 1689 (2002).
37. Wong, H.-W. & Miake-Lye, R. C. Parametric studies of contrail ice particle formation in jet regime using microphysical parcel modeling. *Atmos. Chem. Phys.* **10**, 3261–3272, https://doi.org/10.5194/acp-10-3261-2010 (2010).
38. Unterstrasser, S. Large-eddy simulation study of contrail microphysics and geometry during the vortex phase and consequences on contrail-to-cirrus transition. *J. Geophys. Res. Atmos.* **119**, 7537–7555, https://doi.org/10.1002/2013JD021418 (2014).
39. Schröder, F. et al. On the transition of contrails into cirrus. *J. Atmos. Sci.* **57**, 464–480 (2000).
40. Schröder, F. et al. In situ studies on volatile jet exhaust particle emissions: Impacts of fuel sulfur content and environmental conditions on nuclei mode aerosols. *J. Geophys. Res.* **105**, 941–19,954 (2000).
41. Petzold, A., Döpelheuer, A., Brock, C. A. & Schröder, F. P. In situ observations and model calculations of black carbon emission by aircraft at cruise altitude. *J. Geophys. Res.* **104**, 171–22,181 (1999).
42. Kärcher, B., and Yu, F. Role of aircraft soot emissions in contrail formation, *Geophys. Res. Lett.* **36**, https://doi.org/10.1029/2008GL036649 (2009).
43. Foot, J. S. Some observations of the optical properties of clouds. II: Cirrus. *Quart. J. Royal Meteorol. Soc.* **114**, 145–164 (1988).
44. Unterstrasser, S. & Gierens, K. Numerical simulations of contrail-to-cirrus transition—Part 2: impact of initial ice crystal number, radiation, stratification, secondary nucleation and layer depth. *Atmos. Chem. Phys.* **10**, 2037–2051, https://doi.org/10.5194/acp-10-2037-2010 (2010).
45. Beyersdorf, A. et al. Reductions in aircraft particulate emissions due to the use of Fischer–Tropsch fuels. *Atmos. Chem. Phys.* **14**, 11–23 (2014).
46. Rye, L., Blakey, S. & Wilson, C. W. Sustainability of supply for the planet: a review of potential drop-in alternative aviation fuels. *Energy Environ. Sci.* **3**, 17–27 (2010).
47. Rosenberg, P. D. et al. Particle sizing calibration with refractive index correction for light scattering optical particle counters and impacts upon PCASP and CDP data collected during the Fennec campaign. *Atmos. Measurement Tech.* **5**, 1147–1163 (2012).
48. Borrmann, S., Luo, B. & Mishchenko, M. Application of the T-matrix method to the measurement of aspherical (ellipsoidal) particles with forward scattering optical particle counters. *J. Aerosol Sci.* **31**, 789–799 (2000).
49. Field, P. R. et al. Ice particle interarrival times measured with a fast FSSP. *J. Atmos. Oceanic Technol.* **20**, 249–261 (2003).
50. Noone, K. J. & Hansson, H. C. Calibration of the TSI 3760 condensation nucleus counter for nonstandard operating conditions. *Aerosol Sci. Technol.* **13**, 478–485, https://doi.org/10.1080/02786829008959462 (1990).
51. Rella, C. W. et al. High accuracy measurements of dry mole fractions of carbon dioxide and methane in humid air. *Atmos. Meas. Tech.* **6**, 837–860 (2013).
52. Busen, R. & Buck, A. L. A high-performance hygrometer for aircraft use: Description, installation, and flight data. *J. Atmos. Oceanic Technol.* **12**, 73–84 (1995).

53. Diskin, G. S., Podolske, J. R., Sachse, G. W. & Slate, T. A. Open-Path Airborne Tunable Diode Laser Hygrometer. Diode Lasers and Applications in Atmospheric Sensing. *SPIE Proc.* **4817**, 196–204 (2002).

54. Lance, S. Coincidence errors in a Cloud Droplet Probe (CDP) and a Cloud and Aerosol Spectrometer (CAS), and the improved performance of a modified CDP. *J. Atmos. Oceanic Technol.* **29**, 1532–1541 (2012). Sci., 2010, 3, 17-27.

55. ASTM International. ASTM D7171, Standard Test Method for Hydrogen Content of Middle Distillate Petroleum Products by Low-Resolution Pulsed Nuclear Magnetic Resonance Spectroscopy, ASTM International, West Conshohocken, PA, 2016, www.astm.org 10.1520/D7171-16.

56. ASTM International. ASTM D7566 – 19 Standard specification for aviation turbine fuels containing synthesized hydrocarbons, ASTM International, West Conshohocken, PA, 2019 www.astm.org, 10.1520/D7566-19

57. ASTM International. ASTM D2622, Standard Test Method for Sulfur in Petroleum Products by Wavelength Dispersive X-ray Fluorescence Spectrometry, ASTM International, West Conshohocken, PA, 2016, www.astm.org, 10.1520/D2622-16

58. ASTM International. ASTM D1840, Standard Test Method for Naphthalene Hydrocarbons in Aviation Turbine Fuels by Ultraviolet Spectrophotometry, ASTM International, West Conshohocken, PA, 2017, www.astm.org, 10.1520/D1840-07R17.

Author contributions

H.S., P.L., B.A. and C.V. planned the flight experiment; C.V., J.K., D.S., T.B., R.H.M., S.K., T.J., L.Z., E.C., E.W., M.S., C.R., G.D., J.N., J.D., V.H., Y.B., C.H., S.B., F.H., M.R., B.A. and H.S. performed the in-flight measurements and analyzed the data, P.L., B.R., U.B., M.A. developed the fuel strategy and T.S. analyzed the fuel compositions; J.K., T.B. and C.V. performed the contrail data evaluation, D.S., R.H.M. and B.A. performed the aerosol data evaluation and C.V. wrote the paper with contributions from R.H.M and B.A. All authors commented on the paper.

Competing interests

The authors declare no competing interests.

Additional information

Correspondence and requests for materials should be addressed to C.V.

Peer review information Primary handling editor: Heike Langenberg

Reprints and permission information is available at http://www.nature.com/reprints

Publisher's note Springer Nature remains neutral with regard to jurisdictional claims in published maps and institutional affiliations.